Beam Propagation Studies at NRL
July 1983 to June 1984
Volume 2

R. Hubbard,* M. Raleigh, D. Murphy, R. Pechacek, J. R. Greig, S. Slinker,*
A. W. Ali, J. M. Picone,† J. Boris,† E. Oran,† T. Young,†
R. Fernsler, M. Lampe, S. Hauver and E. Laikin

Plasma Physics Division

*JAYCOR, Inc.
Alexandria, VA 22304

†Laboratory for Computational Physics

AD-A148 198

November 30, 1984

DTIC
ELECTE
NOV 2 7 1984
S
A
D

NAVAL RESEARCH LABORATORY
Washington, D.C.

84 11 26 203

REPORT DOCUMENTATION PAGE

1a. REPORT SECURITY CLASSIFICATION UNCLASSIFIED			1b. RESTRICTIVE MARKINGS			
2a. SECURITY CLASSIFICATION AUTHORITY			3 DISTRIBUTION / AVAILABILITY OF REPORT Approved for public release; distribution unlimited.			
2b. DECLASSIFICATION / DOWNGRADING SCHEDULE						
4 PERFORMING ORGANIZATION REPORT NUMBER(S) NRL Memorandum Report 5412			5. MONITORING ORGANIZATION REPORT NUMBER(S)			
6a. NAME OF PERFORMING ORGANIZATION Naval Research Laboratory		6b OFFICE SYMBOL (If applicable) Code 4792	7a. NAME OF MONITORING ORGANIZATION Naval Surface Weapons Center			
6c. ADDRESS (City, State, and ZIP Code) Washington, DC 20375-5000			7b. ADDRESS (City, State, and ZIP Code) Silver Spring, MD 20910			
8a. NAME OF FUNDING / SPONSORING ORGANIZATION DARPA		8b. OFFICE SYMBOL (If applicable)	9. PROCUREMENT INSTRUMENT IDENTIFICATION NUMBER			
8c. ADDRESS (City, State, and ZIP Code) Arlington, VA 22209			10. SOURCE OF FUNDING NUMBERS			
			PROGRAM ELEMENT NO. 62707E	PROJECT NO.	TASK NO.	WORK UNIT ACCESSION NO. DN680-415

11. TITLE (Include Security Classification)
Beam Propagation Studies at NRL, July 1983 to June 1984, Volume 2

12. PERSONAL AUTHOR(S)
Hubbard, R.,* Raleigh, M., Murphy, D., Pechacek, R., Greig, J.R., Slinker, S.,* Ali, A.W., Picone, J.M.   (Continues)

13a. TYPE OF REPORT Interim	13b. TIME COVERED FROM _____ TO _____	14. DATE OF REPORT (Year, Month, Day) 1984 November 30	15. PAGE COUNT 48

16. SUPPLEMENTARY NOTATION
*JAYCOR, Inc., Alexandria, VA 22304   (Continues)

17.	COSATI CODES		18. SUBJECT TERMS (Continue on reverse if necessary and identify by block number)
FIELD	GROUP	SUB-GROUP	Charged particle beam Beam propagation
			Propagation of CPB DARPA/Services Propagation Review

19. ABSTRACT (Continue on reverse if necessary and identify by block number)

This report is comprised of summaries of unclassified papers presented at the DARPA/Services Annual Propagation Review, June 1984, at the Naval Postgraduate School, Monterey, California. A variety of theoretical and experimental studies are covered, including a review of propagation community codes and topics in channel chemistry, holeboring, hose instability, diagnostics, and beam channel tracking. The papers and authors are listed in the order in which they appeared at the meeting. This report does not include those papers whose first authors were Naval Surface Weapons Center personnel.

DTIC

NOV 27 1984

20 DISTRIBUTION / AVAILABILITY OF ABSTRACT ☒ UNCLASSIFIED/UNLIMITED ☐ SAME AS RPT ☐ DTIC USERS	21. ABSTRACT SECURITY CLASSIFICATION UNCLASSIFIED	
22a. NAME OF RESPONSIBLE INDIVIDUAL M. Lampe	22b. TELEPHONE (Include Area Code) (202) 767-4041	22c. OFFICE SYMBOL Code 4792

DD FORM 1473, 84 MAR   83 APR edition may be used until exhausted.
                              All other editions are obsolete.

12. PERSONAL AUTHOR(S)

Boris, J., Oran, E., Young, T., Fernsler, R., Lampe, M., Hauver, S. and Laikin, E.

16. SUPPLEMENTARY NOTATION (Continued)

CONTENTS

iii

BEAM PROPAGATION STUDIES AT NRL
JULY 1983 TO JUNE 1984
VOLUME 2

Introduction

This report is comprised of summaries of unclassified papers presented at
the DARPA/Services Annual Propagation Review, June 1984, at the Naval
Postgraduate School, Monterey, California. A variety of theoretical and
experimental studies are covered, including a review of propagation community
codes and topics in channel chemistry, holeboring, hose instability,
diagnostics, and beam channel tracking. The papers and authors are listed in
the order in which they appeared at the meeting. This report does not include
those papers whose first authors were Naval Surface Weapons Center personnel.

OVERVIEW OF BEAM PROPAGATION COMPUTER CODES

Richard F. Hubbard

JAYCOR, 205 S. Whiting St., Alexandria, VA 22304

Introduction

Computer modeling has played a major role in the DARPA and Services beam propagation programs. Beam stability and transport involves coupling between complicated plasma physics and air chemistry processes which are not readily treated with purely analytical models. Computer models have been used extensively to provide guidance in choosing design parameters for present and future experiments. They have been particularly useful in suggesting methods for improving beam stability. This paper attempts to provide an overview of computer codes used in the beam propagation program.

Propagation codes rely on approximate treatments of the beam dynamics, fields, and conductivity generation. In most cases, the beam is assumed to be ultrarelativistic and paraxial, so $v_\perp \ll v_z = c$. The frozen approximation, in which z and t are replaced by z and $\zeta = ct-z$, the distance from the beam head, is often made.

A complete nonlinear description in the transformed variables would treat quantities as functions of r, ζ, z, and θ. Most codes either assume $\partial/\partial\theta = 0$ (axisymmetry) or Fourier analyze in θ. In linearized codes, only one Fourier mode (usually m=1) is retained; this is appropriate if deviations from axi-symmetry are small. Channel tracking codes and large chemistry codes are usually static, so $\partial/\partial z = 0$. Certain codes do not calculate radial variations self-consistently (1-D propagation codes) or assume $\partial/\partial\zeta = 0$ (single disc codes).

Basic Components of Propagation Codes

Most beam propagation codes contain modules for treating beam dynamics, conductivity generation (air chemistry), and electromagnetic fields. Over longer time scales, channel hydrodynamics and radiation may also be included.

Beam Dynamics: Axi-symmetric beam dynamics are usually treated with particle simulation, envelope equation, or fluid models. Particle simulation offers the most complete treatment and does not have to rely on ad hoc methods to treat phase-mix damping of oscillation. Codes which treat the resistive hose instability add a dipole (m=1) beam dynamics model. The spread mass and multi-component models partition each beam slice into a number of rigidly oscillating components, while linearized particle simulation models follow the trajectories of a large number of particles.

Field Equations: For models which are not radially resolved, the field equations are usually replaced by a simple circuit model. The most common radially-resolved field equation method uses the ultrarelativistic Lee field equations and the ζ and z variable change. Axi-symmetric, linearized dipole, and fully nonlinear Lee field equation solvers exist at a number of laboratories. The MRC field solvers use the full Maxwell equations and do not make the ultrarelativistic approximation.

Air Chemistry and Conductivity Generation: The simplest conductivity models assume constant momentum transfer frequency ν_m. Most propagation codes now use more elaborate models which calculate $\sigma(n_e, T_e)$ based on rate equations for n_e and T_e or an empirical $T_e(E/\rho)$ relationship. Full air chemistry codes treat z as fixed and treat a large number of atomic and molecular species and rate equations. Nonlocal conductivity codes allow beam generated plasma to be transported and usually focus on the role of energetic secondary electrons (delta rays).

Channel Hydrodynamics: Codes which treat long time scales must allow for channel hydrodynamic motion. Simple adiabatic expansion based on total beam energy deposition is the simplest approach. A radially-resolved 1-D standard hydro package is used in some codes, while the most elaborate hydro treatments are the 2-D and 3-D turbulence models developed at NRL.

Categorization of Computer Codes

In this section, various computer codes will be grouped together in broad categories, and a tabular comparison will be made. Some codes may fall into several categories.

I. Axi-Symmetric Propagation Codes

Code	Lab	Beam Dynamics	Cond	Comments
SIMMO	NRL	Particle	Fixed ν_m	–
RINGBEARERI	LLNL	Particle	Fixed ν_m	–
CPROP	MRC	Particle	$\sigma(n_e, E/\rho)$	Can treat low γ
SIMPAR	LJI	Particle	$\sigma(n,T)$	–
FLUSH	SAI	Fluid	BMCOND	like HIGAP
FLASH	SAI	Fluid	E/ρ+LTE	hydro, radiation
FDFC	LLNL	Fluid		Single disc
APC-2	SNL	Envelope	BMCOND	–
HIGAP	SAI	Envelope	BMCOND	–
EPIC/EBFC	LLNL	Envelope	$\sigma(n_e, T_e)$	hydro, radiation
SPLASH	SAI	Envelope	BMCOND	shower physics

3

These codes can be used to study classical beam transport, nose erosion, and in some cases, axi-symmetric instabilities. Note that most dipole simulations are built upon an axi-symmetric code and can treat the same problems. Fluid models of beam dynamics has received considerable theoretical intention in the past year, but such models have not yet been widely incorporated into propagation codes.

II. Linearized Hose Instability Propagation codes

Code	Lab	Dynamics	Cond.	Comments
VIPER	NRL	multi-comp*	E/ρ+LTE	CPT, channel option
APC-3	SNL	multi-comp*	Fixed ν_m	new code
EMPULSE	LLNL	spread mass*	$\sigma(n_e, T_e)$	CPT option
PHLAP	SAI	spread mass*	E/ρ+LTE	intense beams
SERPENT	AFWL	spread mass*	$\sigma(n_e, T_e)$	inactive
SIMM1	NRL	particle	E/ρ	"coarse grain"
SIMPAR	LJI	particle	$\sigma(n,T)$	orbit averaging
RING-BEARERII	LLNL	particle	Fixed ν_m	inactive
KMRAD	MRC	particle	ζ-indep	arbitrary mode
VALIUM	LLNL	Vlasov	Fixed ν_m	z-indep. equil.

*Assumes self-similar m=0 dynamics (envelope equation)

These have been the "workhorse" codes for the beam propagation program since hose instability considerations often dominate choice of beam and gas parameters. Recent benchmark simulations among VIPER, EMPULSE, SIMM1 have given excellent quantitative agreement for lead pulse ATA hose predictions while providing insight into the role of some subtle conductivity effects. High current beams have also received considerable attention with these codes due to their predicted favorable hose instability properties. Channel tracking, magnetically-coupled multiple pulse modes and extremely long single pulses have also been recently studied with these versatile codes.

III. Nonlinear codes

Code	Lab	Solver	Comments
DYNASTYII	NRL	Dynasty	static; channel tracking
DYNADISC	SNL	"Dynasty"	particle sim.; new code
IPROP	MRC	CPROP mod.	particle sim.; few modes
LEAD	NRL	"Joyce"	lead pulse separation
-	LLNL	"Dynasty"	faster field solver

4

The field solver appears to be the most difficult component of a nonlinear code since convolutions involving many Fourier modes must be evaluated if the deviations from axisymmetry are large. The DYNASTY field solver, which treats the nonlinear Lee equations, is probably too slow for a dynamic code, so considerable effort has been expended in developing faster algorithms. An algorithm developed by Joyce looks particularly promising but is still being tested.

IV. Channel Hydrodynamics Codes

Code	Lab	Dimensionality	Comments
EPIC/EBFC	LLNL	r, ζ, z	Envelope beam
PHAZR	NRL	ζ, limited z	Model turbulence
FLUSH	SAI	r, ζ, z	fluid beam
HINT	NRL	r, ζ	CHMAIR interface
FAST 2D(3D)	NRL	x, y, ζ, (z)	Turbulence studies
HYDRO	LJI	r, ζ	SIMPAR interface

Hydrodynamics codes treat channel motion on long time scales. EPIC and FLUSH have been primarily used to treat long CPT pulse trains and thus must include radiation transport and high temperature chemistry. The other codes have been designed to study the formation of WIPS channels. Note that ζ is the time-like variable in these codes.

V. Beam Conditioning/IFR Codes

Code	Lab	Beam Dynamics	Comments
BEAMFIRE	LLNL	Particle (m=0)	Treats IFR, foil, and air
CENTRING	LLNL	Particle (m=1)	Simpler chemistry
"Wire"	LLNL	Particle	Single disc; external B
"IFR"	SAI	Envelope + rigid displace	For IFR tracking

These codes are designed primarily for wire zone and IFR conditioning cell design. BEAMFIRE predicts the beam radius and emittance of a beam as it emerges into the air from an entrance foil, while the other codes primarily treat electrostatic tracking and damping of transverse oscillations.

VI. Nonlocal Conductivity/Delta Ray Codes

Code	Lab	Method	Comments
Nuts	LLNL	Boltzmann	Relativistic Upgrade
CASK	SAI	Monte Carlo	Emphasizes δ's
LOCHEM	SAI	Multi-fluid;	Ageing model δ's
CPROP	MRC	particle sim.	Also follows beam

Nonlocal conductivity processes can play a major role, especially at reduced pressures. Current multiplication in ETA appears to involve these effects.

VII. Full Air Chemistry Codes

Code	Lab	Comments
CHMAIR II	NRL	Some versions radially-resolved; adiabatic hydro option
HICHEM	SAI	detail balance, high T_g
HITECH	NRL	High T_g version of CHMAIR

This is an abbreviated list of the full scale air chemistry codes discussed in the review by Ali. Such codes are similar in scope to the nonlocal chemistry codes but provide much more detailed treatment of the various air chemistry reactions and species.

Summary

Several important trends have emerged in the past year which should indicate the planned emphasis of code development in the next year. Nonlinear codes are currently under development at LLNL, NRL, SNL, and MRC and are likely to absorb much attention in the future. Magnetically-coupled propagation modes such as CPT are just beginning to receive detailed attention, and the complicated chemistry and radiation processes which accompany such intense beams will require considerable further effort. Fluid beam codes show promise and may also play a major role in the future. Few existing codes can treat the hollow, rotating beam which emerges from RADLAC, but the theoretical foundations for such codes have been developed considerably during the past year. Finally, the approaching propagation experiments on ATA and RADLAC should provide the first real test of the ultrarelativistic codes, and such codes should play a major role in interpreting experimental data and suggesting experimental parameters.

BEAM INDUCED CONDUCTIVITY EXPERIMENTS

M. Raleigh, D.P. Murphy, R.E. Pechacek, and J.R. Greig
Naval Research Laboratory
Plasma Physics Division
Experimental Plasma Physics Branch
Washington, DC 20375

INTRODUCTION

An electron beam ionizes the air through which it passes. This beam induced conductivity in turn determines how the electron beam propagates. How subsequent pulses will propagate is determined by the decay of this conductivity.

In this experiment we have looked for the effect of water vapor on conductivity at early times (< 100 ns) by observing the influence of water content on the net current ($I_{beam} + I_{plasma}$). These measurements have been performed in air and nitrogen with each gas being tested both dry and wet, i.e., with one molecule of water to each 55 ± 5 molecules of air or nitrogen. Pressures of one atmosphere and 40 Torr have been tested. At one atmosphere, one part in 55 represents ~ 60% relative humidity. This ratio at 40 Torr represents the conditions that might exist subsequent to the hydrodynamic expansion of a beam heated channel.

APPARATUS

The beam source is a Pulserad 310 generator driving a cold cathode diode. The diode is coupled to the drift tube via an aluminum transport tube (length 50 cm). Using the transport tube a reproducible 13.5 kA, 1 MeV, 22 ns FWHM beam was injected into the drift tube through a 2.3 cm aperture (Figure 1). The transport tube was always filled with 20 Torr of dry N_2. A small Rogowski coil was mounted just upstream of the titanium foil separating the transport tube from the drift tube. This coil monitored the shot to shot reproducibility of the injected net current.

The drift tube in which the net current measurements were made was an aluminum cylinder 60 cm long by 60 cm in diameter. In a preliminary set of experiments it was determined that the net current would be independent of the drift tube length for lengths over ~ 25 cm and that the net current decreased slightly with increasing drift tube radius for radii over ~ 25 cm. (This is to be expected as a result of the increasing return path inductance.) The drift tube used was choosen large enough to avoid the anomalies associated with the small dimensions but small enough that a lumped inductance would be a good model for the drift tube as a current return path. (Double transit time in the tube ≈ 4 ns, net current risetime ≳ 12 ns.)

For the net current measurements presented here a set of eight equally spaced $\dot{B}$ loops were installed in a shielded groove in the end plate of the drift tube. These loops were summed in parallel to yield a fast (τ_{rise} ≈ 300 ps) Rogowski belt of 25 cm diameter. (A 60 cm diameter Rogowski belt has subsequently been installed and is described elsewhere in the

proceedings of this meeting. The 25 cm diameter belt operates on similar principles.) To both check the calibration of the Rogowski coil and measure the injected REB current (Figure 2), measurements were made using a very short drift tube (~ 3 cm) terminated with a Faraday cup and evacuated to < 1 m Torr.

To supply the various water/gas mixtures to the drift tube a flow-through system was adopted. The gas (water pumped N_2 or zero grade air) was supplied from a regulated cylinder. When wet gas was desired it was passed through a water saturated sponge inside a 15 cm diameter lucite tube. The flow rate and pressure in the lucite tube remained constant regardless of the particular experiment being performed. The gas supply was throttled to the desired pressure as it entered the drift tube. Gas was continuously pumped from the tube through another throttle valve. Bulk flow was maintained through the valves so that the composition of the mixture was not altered. The water content was determined by observing the temperature at which water or ice appeared on a chilled mirror surface.

RESULTS

All net current measurements in the drift tube have been normalized against the average injected net current. Thus the traces shown in Figures 3 and 4 represent average net currents for each condition and may be compared directly with one another. Four or five shots were averaged numerically for each condition and the doted lines show the RMS spread in the data. Since the difference between wet and dry was the same for nitrogen as for air only the results for air are shown.

The following conclusions may be drawn from a comparison of the average net current traces:

1. At 40 Torr in either N_2 or air there is no difference between the gas being wet or dry for the net current during the rising portion of the pulse (0 → 30 ns). There is a slightly higher net current in wet gas during the tail of the pulse, but even this difference is less than the RMS spread in the measurements.

2. At one atmosphere in either N_2 or air the net current peak is higher and occurs later in dry gas. After the current peak the net current is always higher in the dry gas.

3. The net current is slightly less in air than in N_2 under all conditions.

4. For either gas the peak net current is significantly less in 40 Torr than in 1 atmosphere and the decay time is much longer.

ACKNOWLEDGMENT

8

DRIFT TUBE | TRANSPORT TUBE | DIODE

INJECTION CURRENT MONITOR

FARADAY CUP
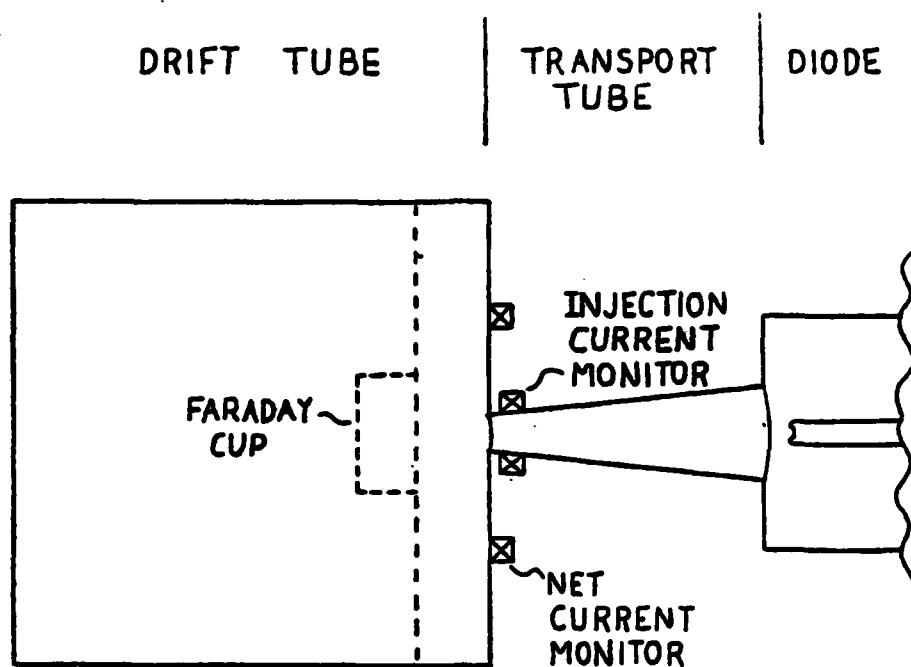
NET CURRENT MONITOR

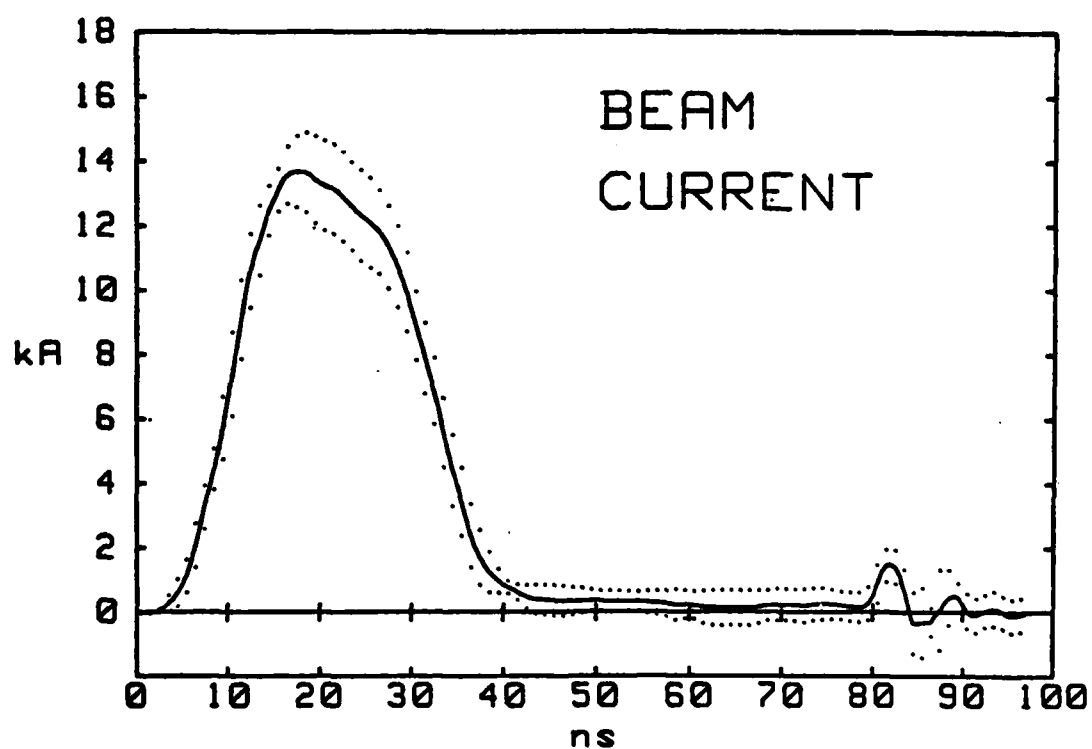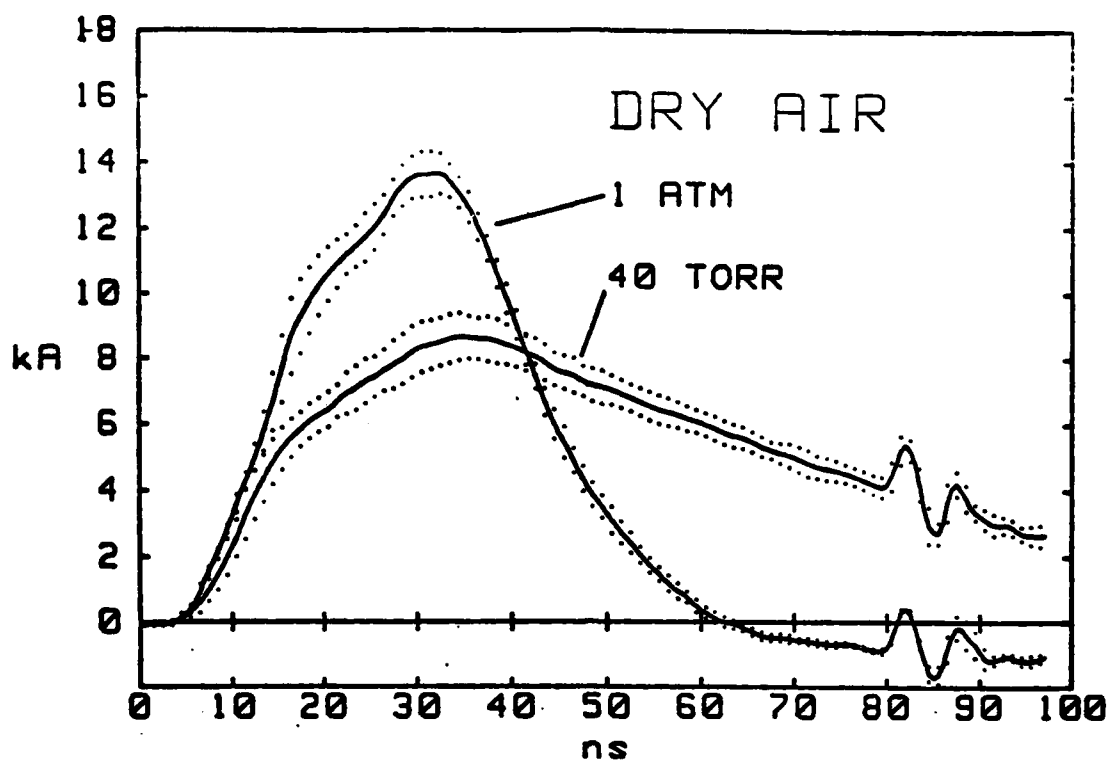FIGURE 1

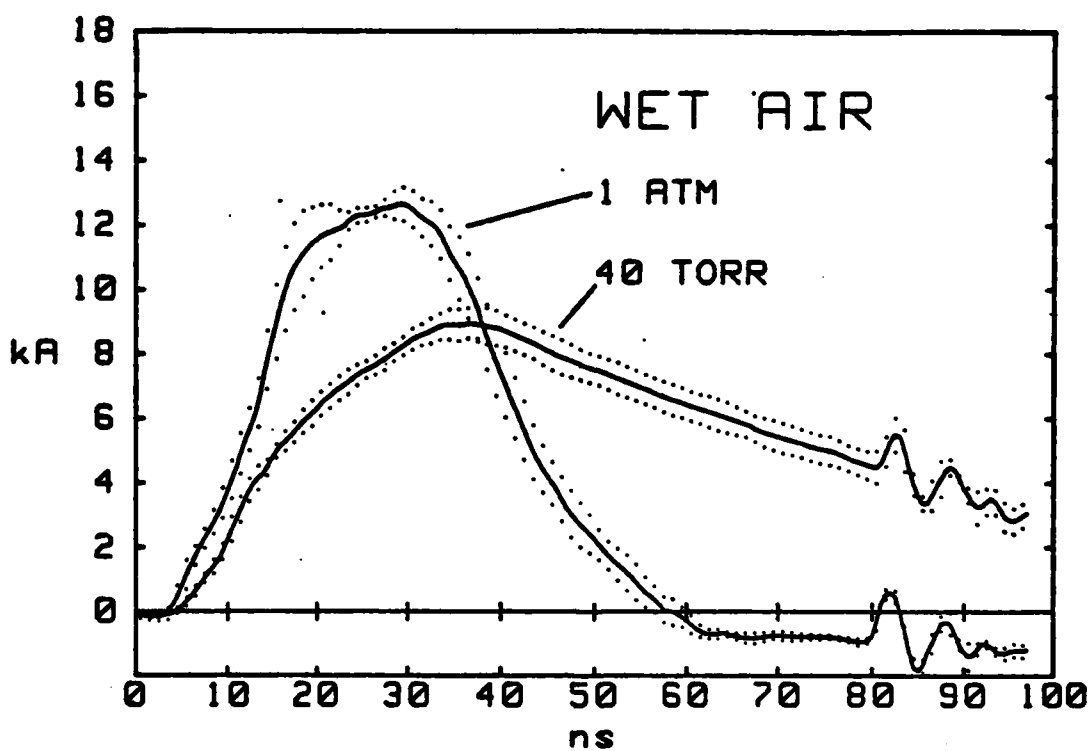BEAM CURRENT

kA

ns

FIGURE 2

FIGURE 3

FIGURE 4

10

On the Vibrational Relaxation and Dissociation of Nitrogen

S. Slinker* and A. W. Ali
Naval Research Laboratory
Washington, DC

1.   Introduction.   There are several reasons why an understanding of the vibrational excitation processes in nitrogen is important for the propagation of an intense electron beam through the air.   On the one hand, the large cross sections for vibrational excitations with plasma electrons means that an appreciable amount of the energy deposited by the beam ends up in vibrations. This keeps the electrons cooler which inhibits ionization and enhances recombination. On the other hand, the relaxation of this energy into the kinetic mode is relatively slow. The rate of release is critical in determining channel formation characteristics. Furthermore, the role of electrons in dissociating the molecules from higher vibrational levels and the complete dissociation of N_2 in high current modes requires a detailed study of the vibrational energy storage and its relaxation.

2. Models and Results.   To illustrate some of these ideas we will give some typical results from runs of the NRL CHMAIR-II code[1] and briefly describe its vibrational energy model. Then we will discuss a detailed nitrogen chemistry code VERAD-II which was developed specifically to address the problems mentioned above.

Tables 1a and 1b show the results in one atmosphere of N_2 using CHMAIR-II. A beam with current of 10 kA, a rise and fall time of 1 ns each and a plateau of 8 ns was utilized for two cases of beam radius R_b = 2 mm and 5 mm.

Table 1a shows several quantities at 5 ns, half way through the pulse. The electron temperature is higher than the vibrational temperature, while the gas temperature is much lower. Roughly 40% of the deposited energy is in vibrational excitation. Table 1b shows the same quantities at 30 ns. By this time the electron and vibrational temperatures are nearly equal and around 60% of the energy is held in the vibrational mode.

*JAYCOR, Alexandria, VA   22304

Beam Radius	$R_b = 2$ mm		$R_b = 5$ mm	
	CHMAIR-II	VERAD	CHMAIR-II	VERAD
VIB.TEMP(eV)	.31	.29	.11	.11
GAS TEMP(eV)	.042	.055	.027	.028
ELEC TEMP (eV)	.45	.45	.32	.32
N-DENSITY	4.8(17)	5.0(17)	6.8(16)	7.0(16)
E-DENSITY	4.5(16)	3.6(16)	1.1(16)	1.1(16)
% ENERGY IN VIB	44	49	37	43
% ENERGY IN HEAT	6	13	5	10

Table 1b.   30 ns

Beam Radius	$R_b = 2$ mm		$R_b = 5$ mm	
	CHMAIR-II	VERAD	CHMAIR-II	VERAD
VIB TEMP(eV)	.78	.65	.18	.16
GAS TEMP(eV)	.065	.090	.030	.034
ELEC TEMP(eV)	.79	.65	.23	.26
N-DENSITY	9.8(17)	1.1(18)	1.6(17)	1.7(17)
E-DENSITY	5.5(16)	2.0(16)	5.8(15)	3.6(15)
% ENERGY IN VIB	65	61	55	54
% ENERGY IN HEAT	6	12	6	13

2.1 CHMAIR-II Model. The vibrational model used in CHMAIR-II is based on the assumption N_2 is a harmonic oscillator and that the vibrational levels are in a Boltzmann distribution characterized by a vibrational temperature T_v due to the rapid excitations and de-excitations by electron impact.[2] The exitation rates[3] are obtained using the measured cross sections.[4] Thus the vibrational energy per molecule, e_v, can be written as

$$\frac{d\, e_v N_2}{dt} = \frac{e_o N_e N_2}{Exp(e_o/T_v)-1} \sum_{i=1}^{8} i X_i \left(Exp(i e_o (T_e - T_v)/T_e T_v) - 1 \right) \qquad (1)$$

where $X_1 = X_1(T_e)$ is the rate for electron impact excitation of 1 quanta, $e \approx 0.3$ eV is the vibrational energy spacing and T_e and T_v are the electron and vibrational temperatures. N_e is the electron density and N_2 is the nitrogen density.

The vibrational relaxation due to heavy particle collisions, e.g., N_2 O_2, and O are added to Eq. 1 independent of electron effects due to different time scales in their collision rates.

2.2 VERAD-I and -II Models.

To ascertain the assumption of the Boltzmann distribution for vibrations and to include the effects of heavy particle collisions on the vibrational levels we developed VERAD-I and -II to describe the vibrational energy and its relaxation using a master equation that solves for 32 levels. Three types of interaction are considered in this model: VE, VT and VV. The VE interactions are the excitation and de-excitation of vibrational levels by electron impact. The VT, vibrational-translational, interactions are those in which a vibrational quantum is gained or lost during a collision with a heavy particle. The VV, vibrational-vibrational, interactions are collisions between nitrogen molecules in which a quantum is exchanged. The details of the master equation for VERAD-I and the appropriate rates can be found in Reference 5.

In VERAD-I we assumed a constant electron density and constant (but not equal) electron and gas temperatures. This model shows the development of the vibrational level distribution which is close to Boltzmann and, hence, verifies the CHMAIR-II model for the vibrational temperature.

VERAD-II solves the master equation including the electron beam interaction with the vibrational levels (including ionization and dissociation). Furthermore, the electron and gas temperatures are calculated from first principles. The ohmic heating is obtained using a circuit equation.

3. Discussion of Results.

Tables 1a and b give the VERAD results for the examples discussed earlier. The vibrational temperature calculated by CHMAIRs-II compares quite well with that of VERAD. VERAD predicts slightly more dissociation. This is consistant with the enhanced dissociation rates of vibrationally excited molecules. The gas temperature predicted by VERAD is higher. The reason is that CHMAIR II carries several of the electronically excited states of N_2 and N whereas VERAD assumes that energy is

13

instantaneously quenched. The electron density in CHMAIR is higher at later times because it uses a more sophisticated collisional-radiative recombination model.

Finally we show one example to illustarte the processes contributing to dissociation and the effect of including quenching due to atomic oxygen. Figure 1a shows the electron, vibrational and gas temperatures of 30 kA, 5 mm beam with a pulse length of 50 ns in pure nitrogen. Though the vibrational and electron temperatures equilibriate soon after the pulse passes, the gas temperature is considerably lower at a microsecond. If we include a fixed amount of 3 x 10^{18} per cc of oxygen atoms, about the amount predicted by CHMAIR for the same beam in air, equilibrium is nearly reached at one microsecond as shown in Fig. 1b. At the end of the run in Fig. 1a the following processes contributions to dissociation were:

direct production of N by the beam	1.1×10^{18} atoms/cc,
production N by dissociative recombination	1.0×10^{18} atoms/cc,
dissociation by secondary electron impact, and	3.1×10^{16} atoms/cc,
dissociation by excitation to 32nd level	2.3×10^{17} atoms/cc.

REFERENCES

1. A. W. Ali, S. Slinker and D. J. Strickland, private communication.

2. A. W. Ali "The Vibrational Temperature of N_2 Due to Electron Impact", Plasma Dynamic's Tech Note #42 (1971). Also NRL Report 7578 (1973). AD 769216

3. S. Slinker and A. W. Ali, "Electron Excitation and Ionization Rate Coefficients for N_2, O_2, NO, N and O", NRL Memorandum Report 4756 (1982). AD A110988

4. G.J.Schulz, Phys. Rev. 135, A988 (1964). D. Spence, J. L. Mauer and G.J.Schulz, J. Chem. Phys. 57, 5516 (1972).

5. A. W. Ali and S. Slinker, Proceedings XVI Int-Conf. Phen. Ion. Gases, Vol. 4, 596, Botticher, Wenk and Schluz-Gulde Eds., Dusseldorf (1983). Also NRL Report in press (1984).
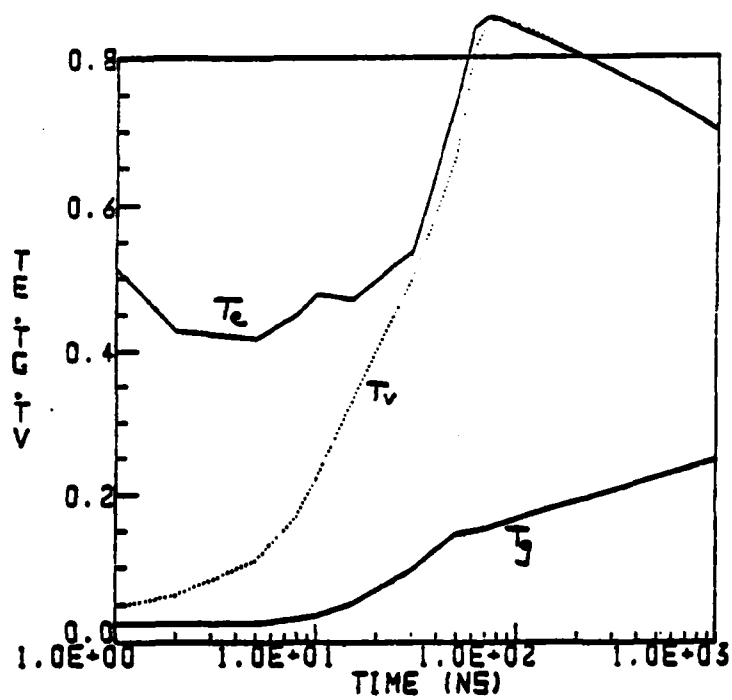
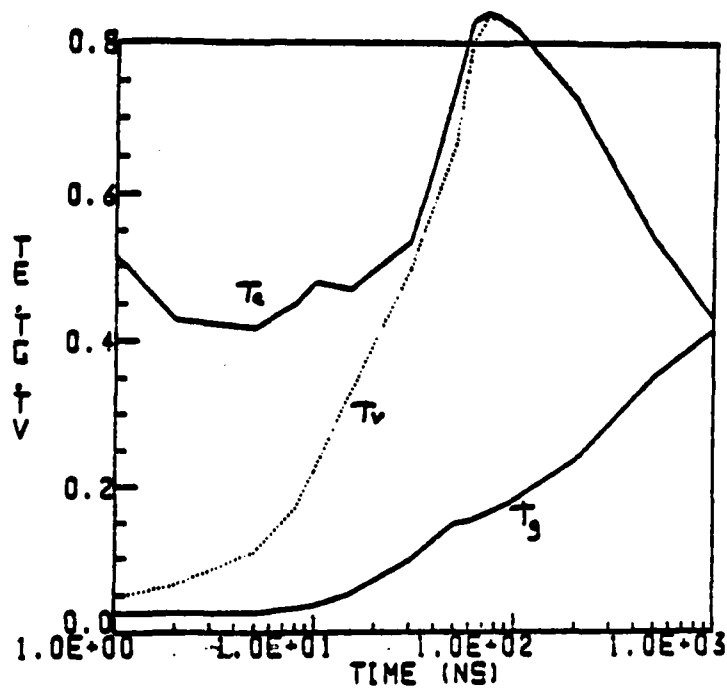Figure 1a. Electron, vibrational and gas temperatures for a
30 kA beam in pure H_2.

Figure 1b. Same as in Fig. 1a in the presence of 3×10^{18}
oxygen atoms.

15

Multipulse Holeboring Calculations with Radially Resolved Chemistry

J. M. Picone, A. W. Ali, S. Slinker,* J. P. Boris,
E. S. Oran, and T. R. Young, Jr.
U. S. Naval Research Laboratory
Washington, D. C. 20375

Introduction

The stable propagation of a multipulse beam over long distances in a gas depends heavily on the hot channel which the beam forms. If the channel quickly reaches a proper balance between gas density and conductivity over the first few pulses, the remaining pulses will be able to reach an equilibrium condition while experiencing a minimum of expansion due to Nordsieck scattering. After a beam pulse has traveled through a given region, a significant fraction of the energy which has been deposited in the gas in that region will reside in molecular vibrational states. To properly model the physics of beam channels, a detailed treatment of nonequilibrium air chemistry is therefore necessary. Toward that end, Ali et al. have developed computer codes for both wet [1] and dry air chemistry [2] and have studied the interactions among the various channel and beam constituents extensively [3]. Recently Ali and Slinker have developed a radially resolved (one-dimensional) version of the CHMAIR II code in order to model channel evolution within a few hundred nanoseconds after a given pulse has passed a point along the beam trajectory.

Also of great importance in modeling the development of the beam channel is the hydrodynamic expansion of the hot gas over a timescale of microseconds following a beam pulse. Such expansion cools the channel between pulses and thus can significantly affect the composition of the channel gas. To account for this, Ali and Slinker incorporated a fluid model based on adiabatic expansion into the zero-dimensional CHMAIR II code and computed channel properties at the axis for a WIPS pulse train [4]. In this paper, we report the development of a radially resolved interpulse air chemistry model in which fluid-dynamic effects are computed using the more rigorous method of flux-corrected transport. After describing the code in some detail, we present a calculation of channel properties for a pulse train with typical ATA parameters. This code should be quite useful in analyzing ATA and RADLAC experiments and the WIPS parameter space.

Interpulse Chemistry Model

Our new model computes the radial distribution of channel properties in a given plane transverse to the trajectory of the beam. The unique feature of the code is the merging of a state-of-the-art compressible flow algorithm (flux-corrected transport [5]) with an appropriate chemical reaction scheme in order to compute the evolution and composition of the channel in detail.

---

*JAYCOR, Alexandria, Virginia

For this reason, we call the code "HINT", which stands for "hydrodynamics and interpulse chemistry." The calculation proceeds by the method of time-step splitting, in which the equations for conservation of mass, momentum, total energy, vibrational energy, and species number are first integrated by flux-corrected transport for a given time step with the chemistry frozen. The resulting values then serve as initial conditions for an implicit integration of the chemical rate equations over the same timestep while the fluid motion is frozen. We currently assume charge conservation in each grid cell in order to compute the electron density, and we set the electron and vibrational temperatures equal. Detailed calculations using CHMAIR II have verified the validity of these assumptions. Currently the code does not account for beam-generated turbulence.

To integrate the chemical rate equations, we use a vectorized version of CHEMEQ [6], which is especially fast and accurate in the nonequilibrium situations characteristic of beam channels. In addition, we use an automatic rate processor to construct the chemical rate equations from literal data, which depict the actual chemical reactions, and numerical data which describe the rate coefficients. Thus, changing the chemical reaction scheme requires no programming, unlike the usual method of hardwiring a specific set of reactions into the chemistry package. In fact, a recent version of the rate processor permits one to enter the temperature equations into the code as a set of pseudoreactions. The various temperatures then become additional species in the reaction scheme.

The interpulse chemistry model currently includes the following variables: gas temperature, vibrational energy per nitrogen molecule, and number densities for N, O, N_2, O_2, NO, NO^+, O_2^-, and e. The interpulse chemistry currently consists of 24 chemical reactions of the following types: neutral association, rearrangement, dissociative recombination, neutral ionization, ion-ion neutralization, attachment, and detachment.

Initial Calculation

To test and calibrate HINT, we have considered a train of five ATA pulses with the following parameters: (1) pulse radius—5 mm, (2) energy—50 MeV, (3) beam current—10 kA, (4) rise time—1 ns, (5) pulse length—10 ns, and (6) pulse repetition interval—30 μs. The calculation begins with a simulation of the first 100 ns by radially resolved CHMAIR II. This time interval is short with respect to the hydrodynamic time scale $r/c_a \sim 10$ μs, so that we would expect minimal error from the exclusion of hydrodynamic motion by that code. The channel conditions at 100 ns serve as initial conditions for the HINT code, which simulates the remainder of the pulse repetition interval. The channel conditions at that time become the initial parameters for the CHMAIR II calculation of energy deposition by the next pulse. In this manner, we attempt to give the most accurate treatment of the two stages of holeboring: energy deposition and hydrodynamic expansion. The results correspond to a position near the nozzle from which the beam exits.

Figure 1 shows mass density versus radius 30 μs after the fifth pulse. The shock waves from this and the previous two pulses are visible at radii

17

of approximately 2.0, 3.0, and 4.0 cm from the center of the channel, and the minimum density is roughly 10 per cent of the ambient value, corresponding to a maximum channel temperature of 0.32 eV. We remark that the channel is not yet at pressure equilibrium with the ambient air after 30 μs; in fact an average overpressure of 0.3 atm still exists. Thus models which assume adiabatic expansion should use an equilibration time scale of about 60 μs for the later pulses.

Figure 2 shows the value of the heavy particle density at the channel axis 30 μs after each pulse and the line gives corresponding values from a recent calculation by Slinker and Ali, in which the gas temperature dropped according to the adiabatic gas law. The latter used CHMAIR II to compute the value of the density only on axis and did not provide radially resolved profiles. The agreement between the two is remarkable, although the HINT channel is slightly cooler, since some of the energy goes into shocks.

Figure 3 shows plots of conductivity on axis versus time after energy deposition for pulses 3, 4, and 5. The aggreement with the calculations of Slinker and Ali is good for pulses 3 and 4 while the axis conductivity computed by HINT is approximately 50 per cent higher for pulse 5. We are still investigating this discrepency at the present time.

The results of this calculation indicate that the HINT code should be quite useful in analyzing channel chemistry and the holeboring properties of particle beams propagating in gases. We will, however, require further testing of the convergence properties of the code under various conditions. We have found, for example, that the code is quite sensitive to the manner in which the vibrational energy is transported and that noise in the pressure is enhanced by the chemistry portion of a timestep. These properties appear to be more important for later pulses, and a thorough study will be necessary to understand the effects of these features on our results.

REFERENCES

1. A.W. Ali, NRL Memo. Rep. 4537 (1981). (AD-A 100619)
2. R.F. Fernsler, A.W. Ali, J.R. Greig, and I.M. Vitkovitsky, NRL Memo. Rep. 4110 (1979). (AD-A 077 667)
3. A.W. Ali, NRL Memo. Reps. 4598 (1981), 4619 (1981), and 4756 (1982).
4. A.W. Ali and S. Slinker, Proceedings of the 1983 DARPA/Service Propagation Review (1983).
5. J.P. Boris and D.L. Book, Math. Comp. Phys. 16, 85 (1976).
6. T.R. Young, Jr., NRL Memo. Rep. 4091 (1980). (AD-A-083-545)
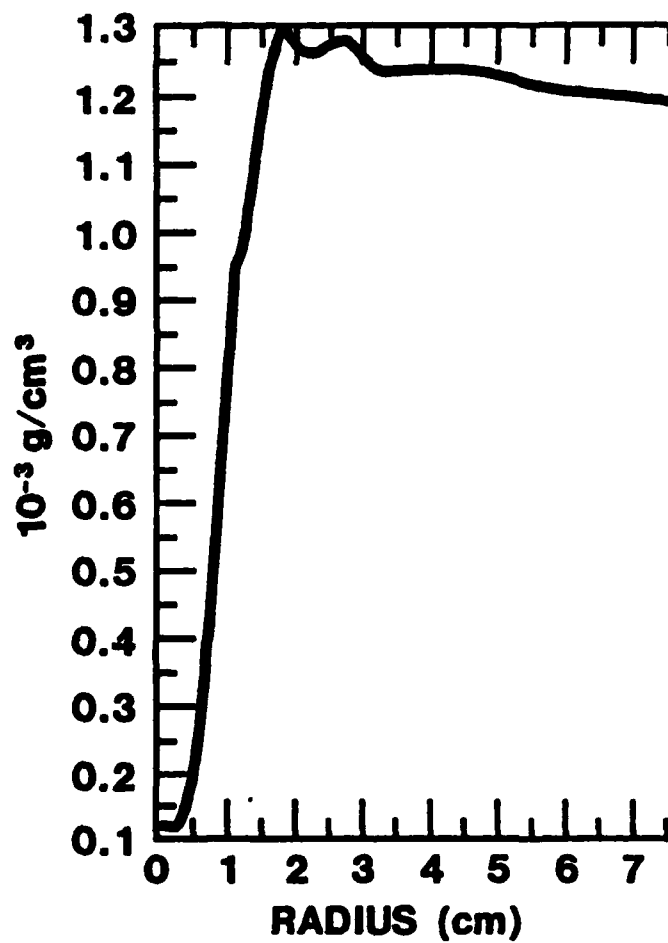
TOTAL MASS DENSITY
30 μs AFTER PULSE 5

Figure 1
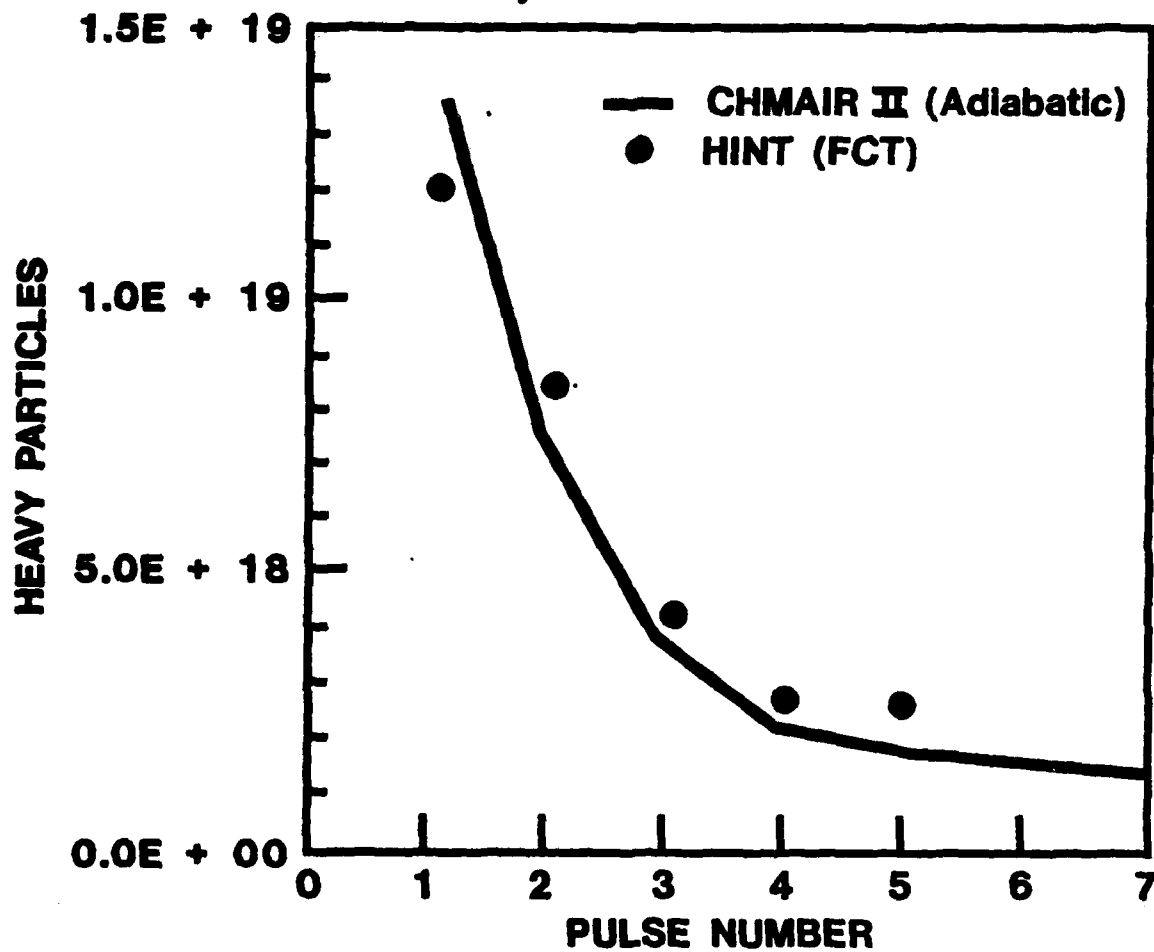
DENSITY ON AXIS
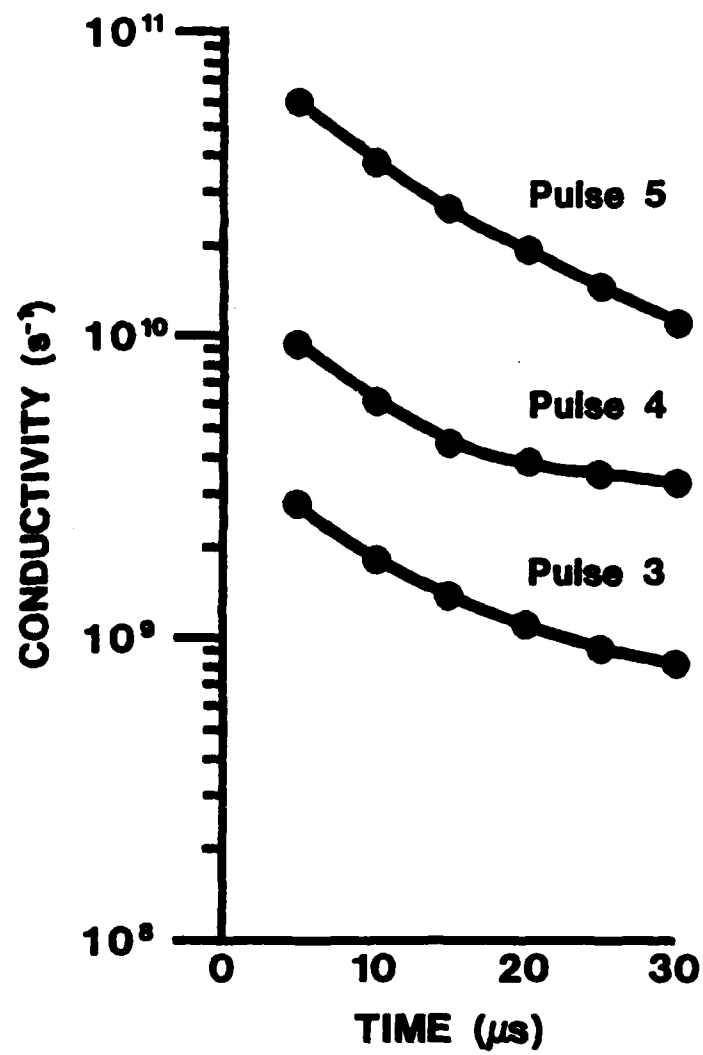**30 μs AFTER PULSE**

Figure 2

20

Figure 3

Effects of Temperature-Dependent Conductivity on Hose

S. Slinker*, R. Hubbard*, R. Fernsler,
A. Ali, and M. Lampe

Naval Research Laboratory
Washington, DC

1. Introduction. In this paper we examine the effects of dipole air chemistry on the resistive hose instability. The main emphasis will be on the variation of the electron neutral collision frequency ν with respect to the electron temperature. This seems to be the most important "exotic" air chemistry effect in the nose of ATA-type beams in full density air. For these beams there is little avalanche ionization. The hose instability is most dangerous in the nose region where the conductivity is low. It will be shown that dipole chemistry effects act to reduce the effective conductivity in this region, thereby allowing the hose to grow more than if these effects were neglected.

2. Collision Frequencies. If $q(v)$ is the cross section for momentum transfer for collisions of electrons of speed v with a species of particle density M and $f(v)$ is the velocity distribution function then the collision frequency, ν, is given by

$$1/\nu = - \frac{4\pi}{3n} \int \frac{v^3}{vqM} \frac{\partial f}{\partial v} \, dv$$

where n is the electron density. If q is constant and f is Maxwellian of temperature T then $\nu \sim MT^{1/2}$. When M is an ion the Coulomb interaction gives $\nu \sim MT^{-3/2}$ if the weak dependence of $\ln\Lambda$ on T and M is ignored. In Fig. 1 we show the collision frequency coefficients for nitrogen, oxygen and air calculated from cross sections compiled in Ref. 1. The typical electron temperature in a beam is on the order of 1 eV. For moderate values of the electric field (we ignore magnetic and ac effects) the conductivity is given by

$$\sigma = \frac{e^2}{m} \frac{n}{\nu} \tag{1}$$

In discharge studies where there is a constant electric field, E, the concept of a drift velocity $v_d = v_d(E)$ is often used. In this case the plasma current density is given by $J = env_d = \sigma E$ so $\sigma = env_d(E)/E$. Although the induced electric field is not constant in intense beams, its variation, for

*JAYCOR, Alexandria, VA 22304

slow rise times, is on the order of a nanosecond while the collision frequency for the plasma electrons is typically 10^{12} in full density air.

3. Effects on Hose.
The collision frequency depends on the electron temperature, which, in turn, depends strongly on the magnitude, E, of the electric field because of ohmic heating. In the following we assume that the collision frequency is a function of E explicitly.

The beam body is the region behind the pinch point but before the region where recombination processes begin to become important. In the beam body Maxwell's equations reduce to Ampere's law[2],

$$-\nabla_{\perp}^2 A = \frac{4\pi}{c} (J_b + J_p)$$

Where A is the axial component of the vector potential J_b is the beam current density and $J_p = \sigma E_z = -\sigma \partial A / \partial \zeta$ is the plasma current density. $\zeta = v_z t - z$ is the distance behind the beam head.

The perturbation of this equation leads to the following equation for the dipole quantities.

$$\frac{\partial}{\partial r} \frac{1}{r} \frac{\partial}{\partial r} r \hat{A} = - \frac{4\pi}{c} (\hat{J}_b + \hat{J}_p) \tag{3}$$

where dipole quantities are denoted by $\wedge$. Using $\nu = \nu(E)$ with $E = |E_z|$ the magnitude of the electric field in (1) the perturbed plasma current becomes, after some algebra,

$$\hat{J}_p = \hat{\sigma} E_z + \sigma \hat{E}_z = \sigma \frac{\hat{n}}{n} E_z - \sigma \{ 1 - \frac{E}{\nu} \frac{d\nu}{dE} \} \frac{\partial \hat{A}}{\partial \zeta} \tag{4}$$

Substituting this in (3) gives

$$\frac{\partial}{\partial r} \frac{1}{r} \frac{\partial}{\partial r} r \hat{A} - \frac{4\pi}{c} \sigma_{eff} \frac{\partial \hat{A}}{\partial \zeta} = - \frac{4\pi}{c} (\hat{J}_b + \sigma E_z \frac{\hat{n}}{n}) \tag{5}$$

where the effective conductivity is defined by

$$\sigma_{eff} = \sigma \{ 1 - \frac{E}{\nu} \frac{d\nu}{dE} \}. \tag{6}$$

In terms of the drift velocity $\sigma_{eff} = en \, dv_d / dE$.

In full density air for the nose of ATA-type beams $d\nu/dE$ is positive (Fig. 1), so the effective conductivity is lower than what it would be if ν were constant. This leads to an expectation of more hose growth and this conclusion is supported by code results from VIPER given in the final section.

23

If ν varies as E^q then $\sigma_{eff} = (1-q)\sigma$. We note in particular that $\sigma_{eff} < 0$ if $q>1$, which can occur for certain ranges of E/p in CH_4 or in Ar doped with C_3F_8. (See Ref. 3 for examples of collision frequencies of various gases.) In this case the hose stability properties are unclear at present, but preliminary investigations indicate that low-frequency modes are damped but high-frequency modes may be unstable (the opposite of the usual situation).

It is also possible for $q<0$, e.g., the Spitzer regime, CO_2. In this case stability should be improved.

There are, of course, monopole effects due to a temperature dependent chemistry model which affect the hose. The higher temperatures in the nose region increase the collision frequency. This will depress the conductivity and cause more hose growth. On the other hand the opposite effect happens in the tail where it is cooler.

The radial profile of the temperature is monotonically decreasing in most cases. In air, this effectively broadens the conductivity which is stabilizing for the hose. This effect is pronounced in density channels where the lower density on axis results in high temperatures.

4. Spread Mass Relation.

Using the spread mass model[2] of Lee, one can derive a dispersion relation equation for the hose when the collision frequency varies as a power of E.

Let $\nu \sim E^q$. If we assume (1) direct beam ionization is the only source of electrons, (2) the return current fraction $f = I_p/I_b$ where I_p is the plasma current is fixed and (3) the radial profile of σ and J_b are Bennett with the same radius, then the electric field is determined,

$$E = \left(\frac{|\sigma|}{\kappa\zeta}\right)^{\frac{1}{1-q}}$$

where κ is a constant.

The spread mass model assumes $\hat{A} = -(dA/dr)D$ and $\hat{J} = -(dJ/dr)D(1+G)$ where all the ζ dependence is in D and G is a function of Ω^2 and $\Omega^2_{\beta 0}$ where Ω is the z-frequency of the disturbance and $\Omega_{\beta 0}$ is the on-axis betatron frequency. Making these substitutions results in

$$\left(1 + \zeta\frac{\partial}{\partial\zeta}\right)\left(1 + \lambda_q \zeta^{\frac{1}{1-q}}\frac{\partial}{\partial\zeta}\right)D = \frac{1+G}{1+f}\left(1 + f + \zeta\frac{\partial}{\partial\zeta}\right)D \qquad (7)$$

where

$$\lambda_q = \frac{\kappa I_b}{2c} (1-q)(\frac{|\zeta|}{\kappa})^{\frac{-q}{1-q}} .$$

The case q=0 has been solved in Ref. 4.

5. Code Results. In this section we present VIPER code results illustrating the theory. The collision frequency used in VIPER is the sum of the electron-neutral collision frequency of Fig. 1 and the Spitzer term. The electron temperature in eV is given by an E/P model;

$$T_e = 0.1(E/P)^{0.8} + T_o$$

where E/p is in volts/cm/torr and T_o is a constant modeling the direct beam heating. The other term was derived by Ali[5] from ionization rates.

Figure 2 shows the maximum hose displacement (saturation had not occurred by the time of the graph) as a function of ζ for a 10 kA, 5 mm beam. The three curves correspond to three VIPER runs. In A the full dipole conductivity terms are retained. In B the dipole conductivity is set equal to zero. In C only the contribution to $\hat{\sigma}$ due to $\hat{n}$ is retained. As seen in the figure this part of the dipole conductivity is stabilizing. This is explained in Ref. 4. The inclusion of the ν term, Case A, is seen to be destabilizing in accordance with theory.

Finally, Fig. 3 shows the on-axis conductivity, σ, electric field and fraction σ_{eff}/σ as a function of ζ. For this beam the conductivity is reduced by nearly 50% in regions where the hose is dangerous.

References

1. See, e.g., A. W. Ali, NRL Memo Report (in press), and references therein.
2. E. P. Lee, Phys. Fluids 21, 1327 (1978)
3. For example, L. G. Christophorou, et al., Appl. Phys. Lett., Vol. 41, No. 2, 147 (1982).   Y. Itikawa, Phys. Fluids, Vol. 16, No. 6, 831 (1973).
4. M. Lampe, W. Sharp, and R. Hubbard, NRL Memo Rpt. 5140 (1984). (AD-A137 549)
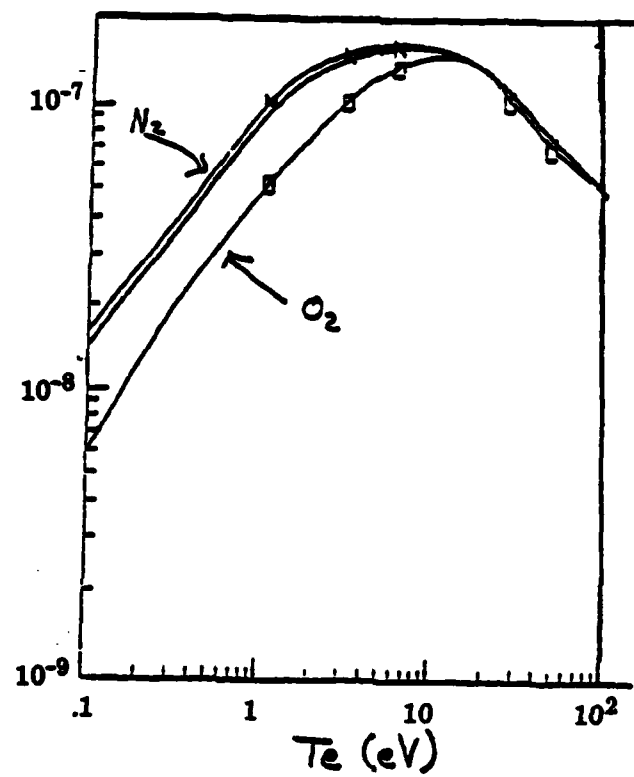5. A. W. Ali, NRL Memo Rpt. 4794 (1982). (AD-A113501)

Fig. 1 — v/M (cm^3/sec) for N_2, O_2 and air

A: $\hat{\sigma} = \sigma\left(\frac{\hat{n}}{n} - \frac{\hat{v}}{v}\right)$

B: $\hat{\sigma} = 0$

C: $\hat{\sigma} = \sigma\frac{\hat{n}}{n}$
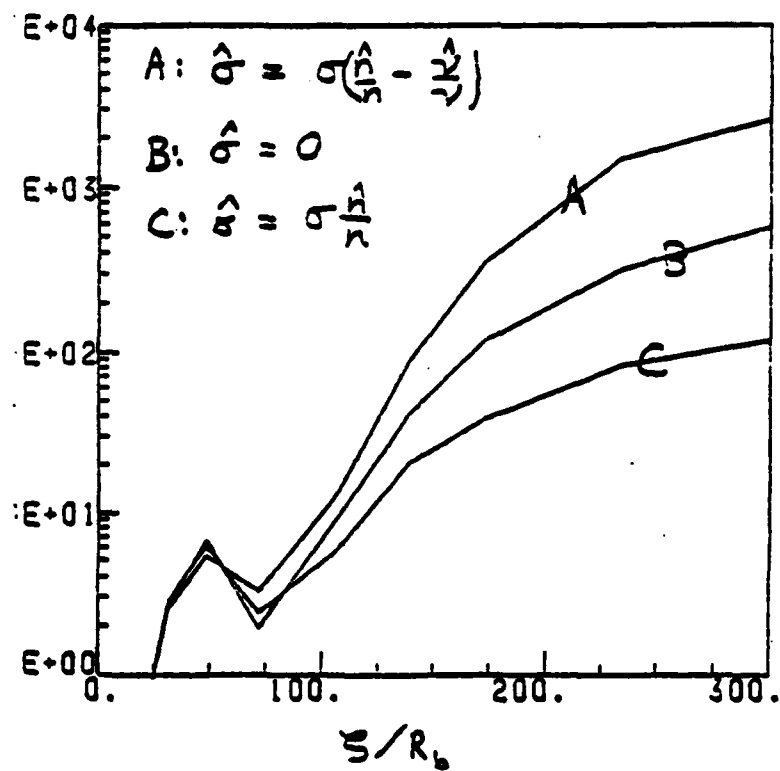
ς/R_b

Fig. 2 — Maximum hose growth for 10 kA, 5 mm beam
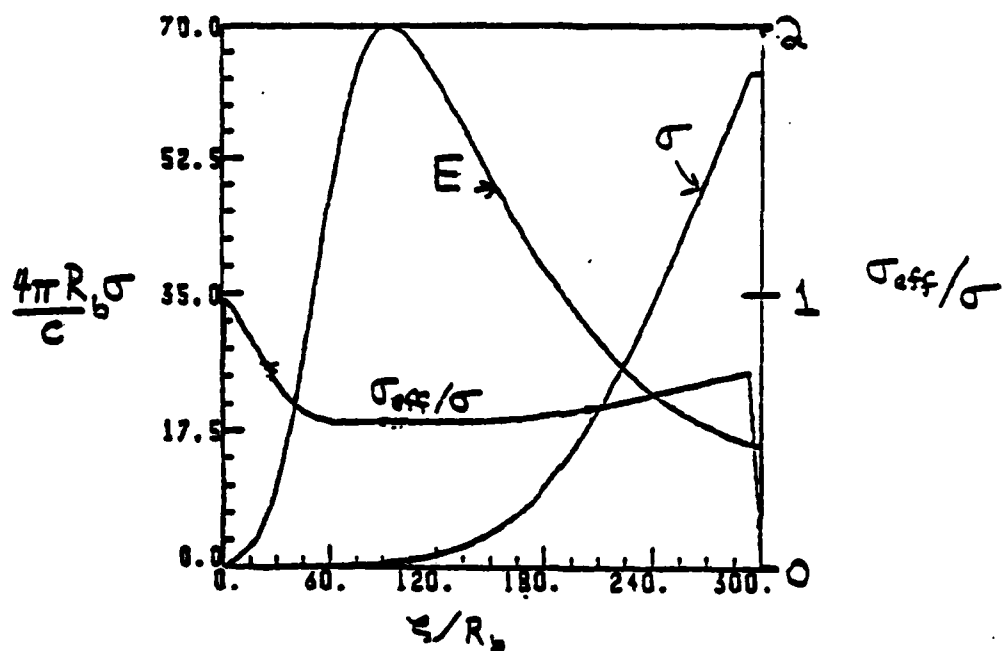with risetime of 200 beam radii.

Fig. 3 — On-axis electric field, conductivity and conductivity ratio for Case A in Figure 2. The maximum electric field is 9000 v/cm.

DIAGNOSTIC DEVICES

M. Raleigh, R.E. Pechacek, S. Hauver, D.P. Murphy, and J.R. Greig
Naval Research Laboratory
Experimental Plasma Physics Branch
Plasma Physics Division
Washington, DC 20375

INTRODUCTION

During the course of our CPB propagation experiments we have found it necessary to design a number of rather simple, but none the less effective and useful, diagnostic systems. In this manuscript we describe first a single frame, gated, image intensified camera and then some very fast B-dot loops that are back terminated so that several of them can ganged together to produce super-fast Rogowski belts or devices sensitive to the position of the current centroid. These are not new inventions but rather conveniently packaged versions of well known devices for which working drawings are available.

THE GATED MICROCHANNEL PLATE REFLEX CAMERA

The original purpose of this camera was to make it possible to photograph a typical REB/atmosphere interaction in the presence of a preformed luminous channel. The camera (Figure 1) consists of a standard Hasselblad 500/C camera with a Polaroid film back which has been modified so that a proximity focussed microchannel plate intensifier tube (ITT F4111) is positioned between the film plane of the camera and the Polaroid film. This intensified tube has been gated to exposure times of a few nanoseconds[1] and as mounted in this camera should be capable of exposure times as low as ~ 10 ns. So far we have demonstrated exposure times down to ~ 25 ns. The frame size is a circle ~ 1 cm diameter and the optical gain of the system is ~ 1000.

The image intensifier package consists of three parts: a metal adapter plate that mates with a Hasselblad 500/C, an aluminum housing that contains the intensifier tube, and a standard plastic Polaroid film pack holder. The adapter plate and the film pack holder are parts from a standard 500/C Polaroid back. In its operating position, the image tube photocathode is located at the image plane of the lens and the output fiber-optic plate is pushing gently against the Polaroid film. The film pull-tabs are covered by a lever. Pulling the lever to uncover the pull-tabs also moves the intensifier tube away from the film allowing the film to be pulled without wiping on the fiber-optic plate. A scene to be photographed through the image intensifier is focussed through the reflex optics of the camera. No continuous operation 'focus' mode is necessary for the image intensifier. Further, by replacing the image intensifier package with a Polaroid film back, the scene can be photographed directly for alignment or reference purposes. Lastly, this image intensifier system has the advantage of a complete camera system: a variety of commercially available accessories and a large variety of lenses each with its own mechanical shutter and iris.

SIMPLE B-DOT LOOPS AND ROGOWSKI BELTS

Two specific B-dot loops have been used at NRL. (Figures 2b and 3b). The larger loop (Figure 2b) has an area of ~ 5 cm^2 and is a single turn loop almost totally enclosed in 3/16 inch soft copper pipe. The loop is "back terminated" as shown with a 50 Ω resistor to prevent reflections when several (typically eight) of these loops, situated around the circumference of a circle, are used with the summing network shown in Figure 2a to form a Rogowski belt. The risetime of these loops and of the 60 cm diameter Rogowski belt containing eight loops is ~ 750 ps.

The smaller loop (Figure 3b) has an area of only ~ 0.5 cm^2, is a single turn loop, and is embedded as indicated in a block of aluminum. Again the loop is "back terminated" with a 50 Ω resistor so that the outputs for several loops can be summed to form a Rogowski belt. In this case four or eight such loops are embedded in a circular groove cut in an aluminum end flange (Figure 3a) through which the REB is made to propagate. These loops and their Rogowski belts have a measured risetime of ~ 250 ps. Four loop belts on a 5 cm diameter and eight loop belts on a 25 cm diameter have been used.

When these Rogowski belts are used in conjunction with our fast integrators (NRL Memorandum Report No. 4939 (1982)) which have a risetime of ~ 300 ps, net current measurements can be made with time resolution compatible with that achieved with a Tektronix 7104 oscilloscope, i.e., a total system risetime of ~ 500 ps.

ACKNOWLEDGMENT

REFERENCES

1. N.P.S. King, G.J. Yates, S.A. Jaramillo, J.W. Ogle, J.L. Detch, Jr., Los Alamos Scientific Laboratory Report LA-UR-81-1126.
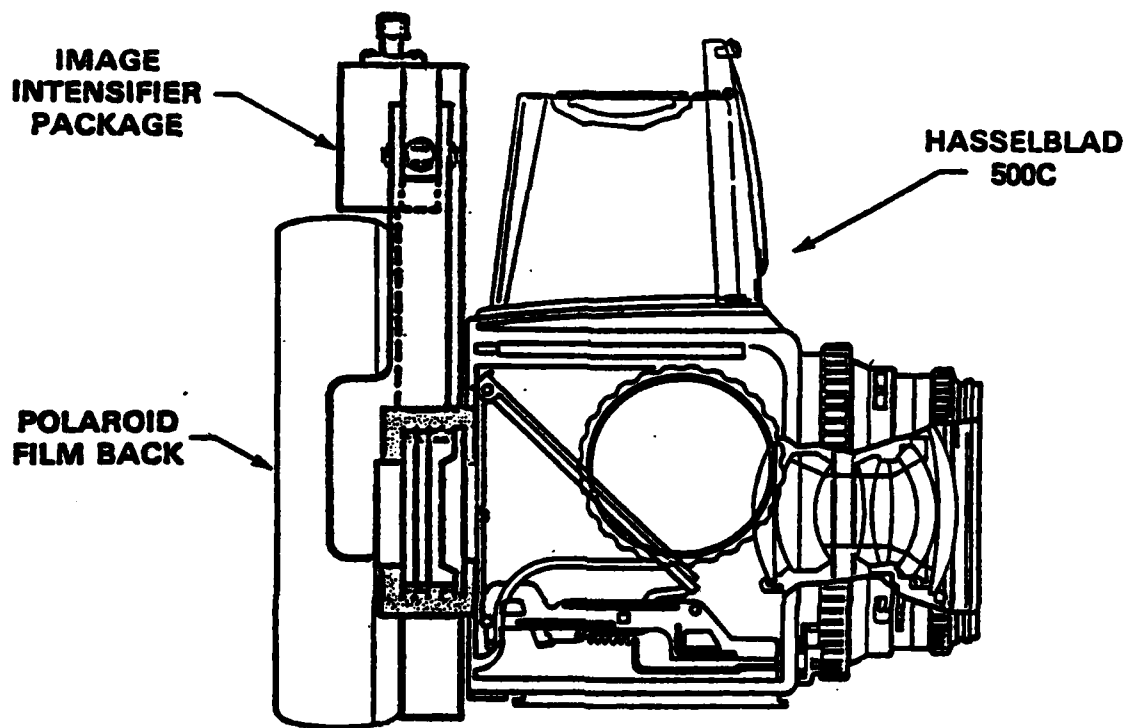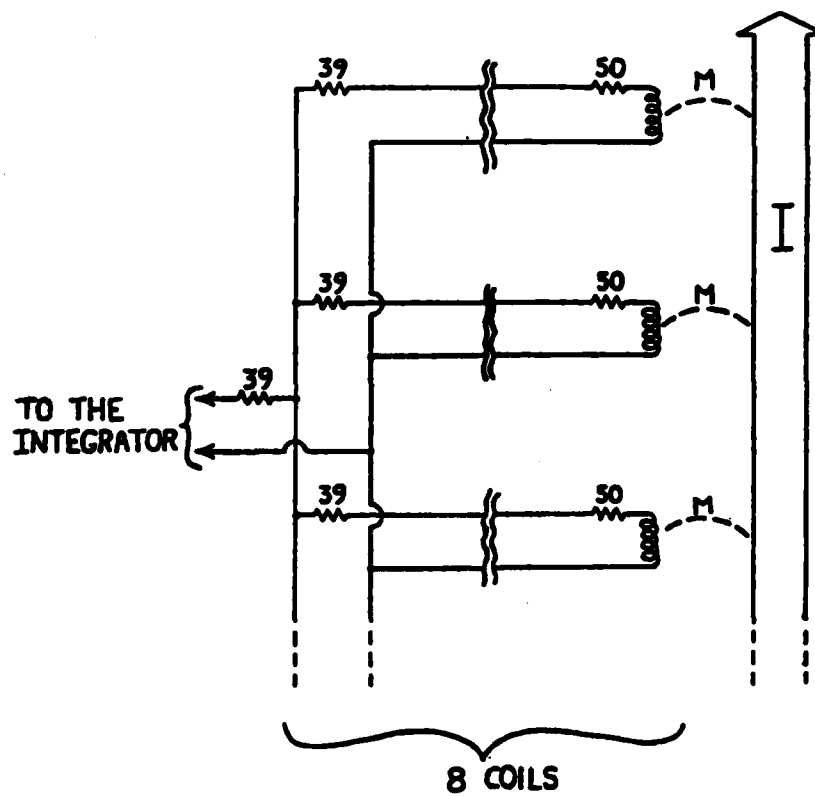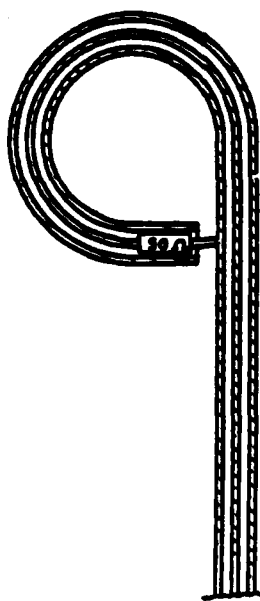
IMAGE
INTENSIFIER
PACKAGE

HASSELBLAD
500C

POLAROID
FILM BACK

FIGURE 1

31

TO THE
INTEGRATOR

8 COILS
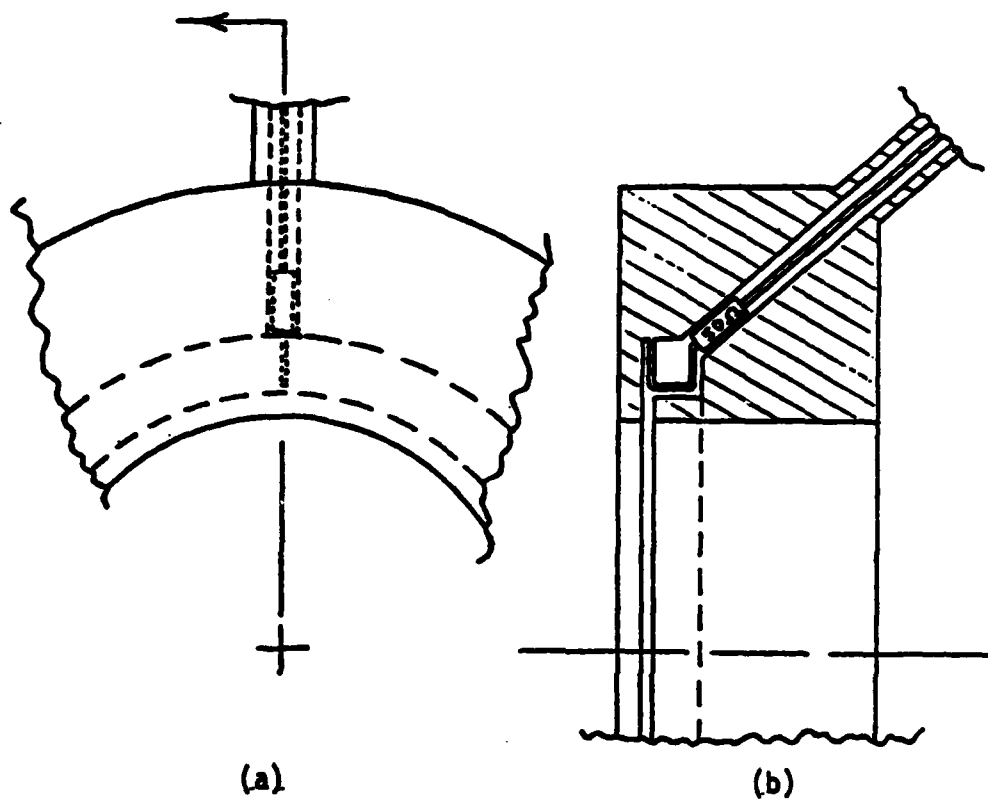
(a)

(b)

FIGURE 2

32

(a)　　　　　　　　(b)

FIGURE 3

THE DIAGNOSTICS OF HIGH CURRENT GENERATED AIR PLASMAS

A. W. Ali, Naval Research Laboratory, Washington, D. C.

1. INTRODUCTION

The propagation of a high current electron beam in air is accompanied by the air plasma and the heating of air. Thus a channel is generated with numerous properties that control the propagation and the guidance of the beam. These properties are time and space dependent and depend on various properties of the beam current. In general, however, one can divide the channel characteristics into four distinct time scales; which are, the early time, the saturated region, the beam turn off region and the late time. The properties of the plasma and the channel, such as the conductivity, etc., are important parameters which must be determined over the entire time scale for a comprehensive understanding of the channel physics.

In this paper we discuss the measurements of several spectroscopic quantities which will provide quantitative answers to the channel properties of interest for a high temperature plasma.

2. CHANNEL PLASMA PROPERTIES

The following quantities are considered as important channel properties to be determined: (a) The conductivity, (b) The electron density, (c) The electron temperature, (d) The degrees of ionization and dissociation, (e) The heavy particle temperature and (f) The vibrational temperature.

These quantities can be obtained from certain spectroscopic measurements discussed in the next section.

3. SPECTROSCOPIC MEASUREMENTS

We propose the time resolved and space resolved meansurements of the following quantities:

(a) The intensity at 3371Å and 3914Å from N_2 and N_2^+

(b) The intensity and the Stark width of 5330Å and 6157Å from oxygen atom

(c) The intensity and the Stark widths of 4222Å and 4256Å from nitrogen atom

(d) The intensity and the Stark width of one or more of these lines at 4913Å, 4341Å, 4111Å, 4074Å and 3966Å from oxygen ion (O^+)

(e) The intensity and the Stark widths of one or more of these lines at 4613Å, 4643Å, 5006Å, 4447Å and 3995Å from nitrogen ion (N^+)

(f) And the intensity of a 20Å band continuum emission at 4834Å

These intensities and widths provide abundant information on the electron density, electron temperature, atomic and molecular densities and the densities of their respective ions.

4. CALCULATIONS OF THE MEASURED QUANTITIES

The Stark widths for the lines suggested above have been calculated and measured for specific electron densities and temperatures. Their data can be interpolated or extrapolated for any desired electron density.

The lines, bands and the continuum intensities can be calculated using detailed abinitio electron energy deposition, air chemistry and emission codes. Some typical continuum calculations are presented for several plasma temperatures in Figures 1, 2 and 3 where the free-free (electron-ion), the free-bound, and the free-free (electron-neutral) emissions are shown. In Figure 3 indications are given for band emissions from NO, H_2O and CO_2 in the infrared region which will be superimposed over the calculated continuum. These band emissions can be calculated by the knowledge of the species densities, the vibrational and the gas temperatures in the channel provided by air chemistry models.

5. CONCLUSIONS

With a redundant information, from the spectroscopic measurements, on the electron density, electron temperature and species densities, a chanllenging opportunity arises for the code-experimental data analysis and interaction.
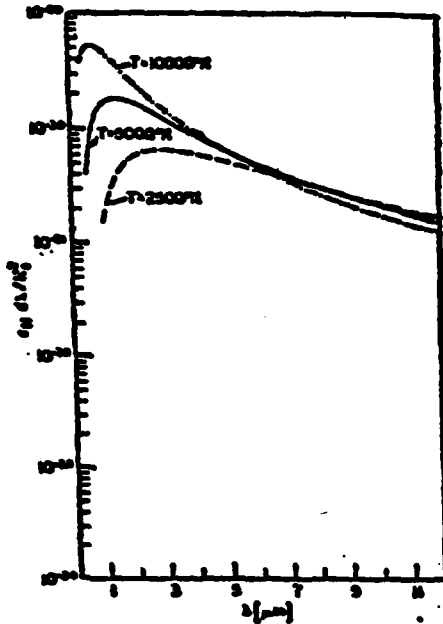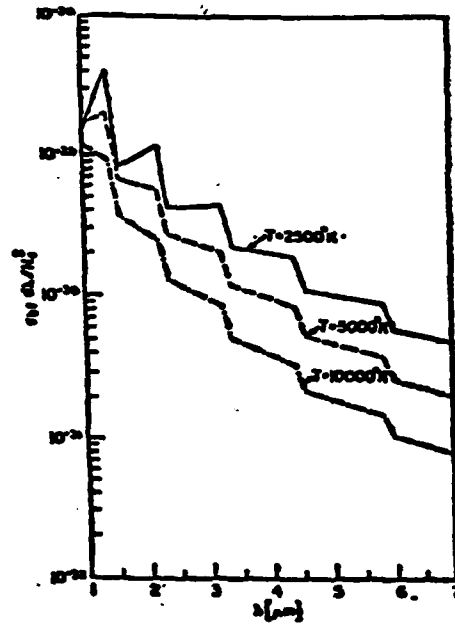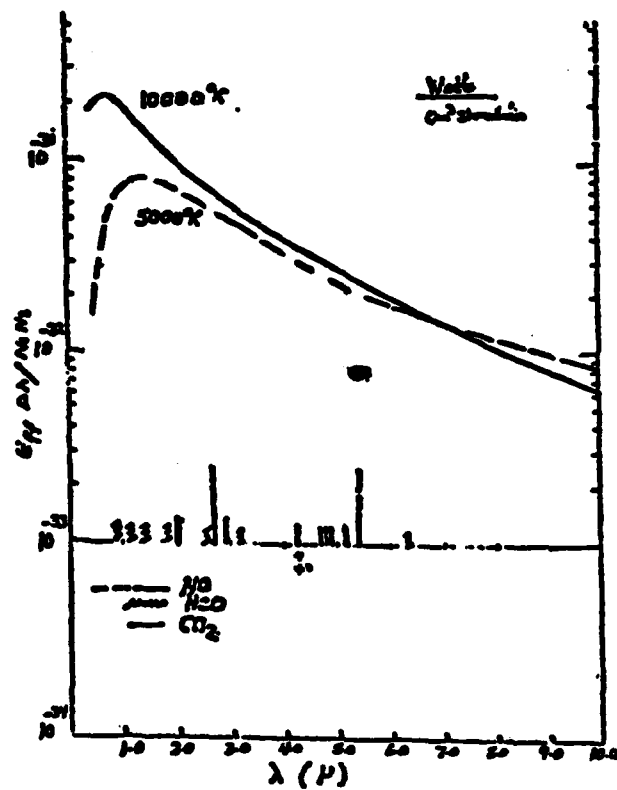

Figure 1

Figure 2

Figure 3

REB/CHANNEL TRACKING EXPERIMENTS IN LOW PRESSURE AMMONIA

D.P. Murphy, M. Raleigh, R.F. Fernsler, E. Laikin,
R.E. Pechacek and J.R. Greig
Naval Research Laboratory
Plasma Physics Division
Experimental Plasma Physics Branch
Washington, DC 20375

ABSTRACT

We describe an experiment in which an intense REB has been allowed to interact with reduced density channels in ammonia at an ambient pressure of 40 Torr. Ammonia was chosen for these experiments because of its ability to absorb the energy from a pulsed CO_2 laser. This permitted the formation of reduced density channels in an otherwise uniform atmosphere of ammonia. At this pressure and with these particular REB characteristics, avalanche ionization was not a major source of plasma conductivity in the ambient gas. But in the reduced-density channel and using high inductance boundary conditions avalanche ionization was the major source of plasma conductivity, easily exceeding beam induced conductivity (i.e., by direct particle collisions). Then the presence of the reduced-density channel significantly influenced REB propagation. Plasma return currents were markedly increased and confined to the channel with the result that the REB was always expelled/repelled from the channel.

APPARATUS

These propagation experiments were performed in a large test chamber made of fiberglass. The chamber was cylindrical: 1.5 m long and 0.6 m in diameter (Figure 1). The chamber could be fitted with a brass conducting liner to change from the initial nonconducting wall boundary conditions to conducting wall boundary conditions. The CO_2 laser beam entered the test chamber through a salt (NaCl) window on the end of a 2.5 m long extension tube. Further details are available in NRL Memorandum Report #5281 (1984).

CHANNEL AND REB CHARACTERISTICS

To create reduced density channels in the ammonia gas a 10 m focal length, salt lens focused the CO_2 laser beam through a circular aperture on the salt window that clipped the laser beam to a 2 cm radius spot where the REB entered the test chamber. The heated gas expanded to form a simple channel of radius ~ 2.5 cm (Figure 2).

Because the effects of absorption and focusing were nearly matched, the laser energy deposited in the ammonia gas was fairly uniform at ~ 25 mJ/cm^2 along the length of the channel. This amount of energy (~ 0.1 eV/molecule) while several times the ambient energy (~ 0.025 eV/molecule) was negligible compared to the dissociation potential (4.3 eV) and the ionization potential (10.15 eV) of ammonia.[1]

The vibrational-translational relaxation of the excited ammonia molecule is very fast,[2] ~ 100 ns at a pressure of 40 Torr. Thus we expected channel formation to result from effectively instantaneous thermalization followed by relaxation, on hydrodynamic time scales, to pressure equilibrium. We did not expect the laser to generate any conductivity in the channels.[3] These aspects of the channel history were confirmed using double exposure holographic interferometry[4] and an RF bridge[5] respectively.

The Pulserad 310 generator produced an REB of approximately 19 kA peak current at
1.1 MV peak voltage with a pulse width of 26 ns FWHM. The REB was transported to the
test chamber through a drift tube containing a conical return current conductor and
filled with dry nitrogen at 20 Torr. It entered the test chamber through a 2.3 cm
aperture. The peak REB current entering the test chamber was ~ 8 kA and it had the
current density profile shown in Figure 2.

EXPERIMENTAL RESULTS

The REB was injected into the test chamber under four distinct experimental
conditions:

        (i) conducting liner installed - no channel present
       (ii) conducting liner installed - channel present
      (iii) conducting liner removed - no channel present
       (iv) conducting liner removed - channel present.

The time histories for the measured REB and net currents along with the calculated
plasma current are shown in Figure 3 for case (i). Note that the plasma current was
negative during much of the REB pulse. In all four cases the REB failed to propagate
the length of the test chamber and deviation from its initial trajectory increased with
each case: (i) through (iv). We were able to correlate the magnitude of the deviation
with a parameter we call f^* where

$$f^* = 1 - \frac{(I_N)_{max}}{(I_B)_{max}} .$$

Case	f^*	REB Behavior
i	~ .3	Moderate hosing
ii	~ .3	Moderate hosing
iii	~ .5	Violent hosing
iv	~ .7	REB dispersed

ANALYSIS

The conductivity of the gas in the chamber is a function of the electron density
and the gas density, $\sigma = \sigma(n_e/n)$. The growth of conductivity was governed by the
production rate of electrons generated by the passage of the REB through the gas. Four
contributions to the rate equation were direct collisional ionization, avalanche
ionization, dissociative attachment and dissociative recombination,

$$\dot{n}_e = \frac{1}{\chi} \frac{d\epsilon}{ds} \frac{J_B}{e} + \alpha \, n_e - \eta n n_e - \beta n_e^2 . \qquad (1)$$

These four terms are implicit and/or explicit functions of the gas density, n, the
electron density, n_e, the electric field, E, and the REB current density, J_B. The
avalanche ionization coefficient, α, is in particular a very strong function of the
density normalized electric field, E/n. Figure 4 is a plot of the density normalized
avalanche coefficient, α/n, as a function of E/n for both air and ammonia.[3,6] The
avalanche coefficient increases if either the gas density drops, as in a channel, or
the electric field increases. Our REB, when injected into the lined test chamber with
40 Torr ammonia present produced an initial density normalized electric field
of ~ 200 Td. This same REB injected into a reduced density channel would develop a
larger density normalized electric field of ~ 800 Td.

Being in the limit where the risetime of the REB was longer than any transit time for electromagnetic waves within the test system, the electric field generated by the REB was $E = L \dot{I}_N$ where I_N is the net current and L is the inductance per unit length seen by the REB. When the test chamber was lined with a conducting screen this lumped circuit inductance was estimated to be that for two concentric coaxial cylinders of radii a = 1.2 cm and b = 30 cm,

$$L = L_c = \frac{\mu_0}{2\pi} \ln(\frac{b}{a}) = .5\mu_0 \ (H/m) \quad . \tag{2}$$

The test chamber sat in a metal walled room of 3 x 3 m cross section. When the screen liner was removed from the test chamber the outer conducting boundary radius, b, defaulted to that of the metal experimental room, b ~ 150 cm. The estimated lumped circuit inductance for the nonconducting test chamber was L_{nc},

$$L = L_{nc} = \frac{\mu_0}{2\pi} \ln(\frac{150}{1.2}) = .8\mu_0 \ (H/m) \quad . \tag{3}$$

Since $L_{nc} > L_c$ the density normalized electric field, E/n, was larger when the conducting liner was removed from the test chamber.

We developed a computer model of the REB/plasma interaction from a simple lumped parameter circuit model. The model used the measured time history of the REB, the channel parameters and the boundry conditions to calculate the plasma and net currents. The model predicted values of f^* very close to those actually measured in the experiment for sets of parameters that matched the true experimental conditions.

The effect of changing the experimental conditions was to alter the relative importance of the terms in the rate equation. For example, in case (iv), the avalanche ionization rate in the channel was increased by approximately two orders of magnitude over case (i) and dominated the other terms in the electron rate equation. The model predicted a large increase in the channel conductivity and a very localized plasma return current, exactly as observed in the experiment.

CONCLUSION

We have injected an intense REB into a test chamber filled with 40 Torr ammonia gas and observed the effect of boundary conditions and reduced density channels on the propagation of the REB. We have also shown that a simple computer model of the interaction accurately forecasts the most important macroscopic parameters of the interaction.

Under the conditions of an enhanced density normalized E field, such as in case (iv) where $f^* \sim .7$, propagation of the REB was completely disrupted with the REB striking the chamber walls within 30 cm of injection. When the experimental conditions were adjusted so the avalanche term was less dominant ($f^* = 0.3$ to 0.5) the REB was again ejected from the channel and was hose unstable but did not break apart. At no time did the simple density channels attract or guide the REB; their effect was always disruptive.

REB/CHANNEL INTERACTION TEST CHAMBER
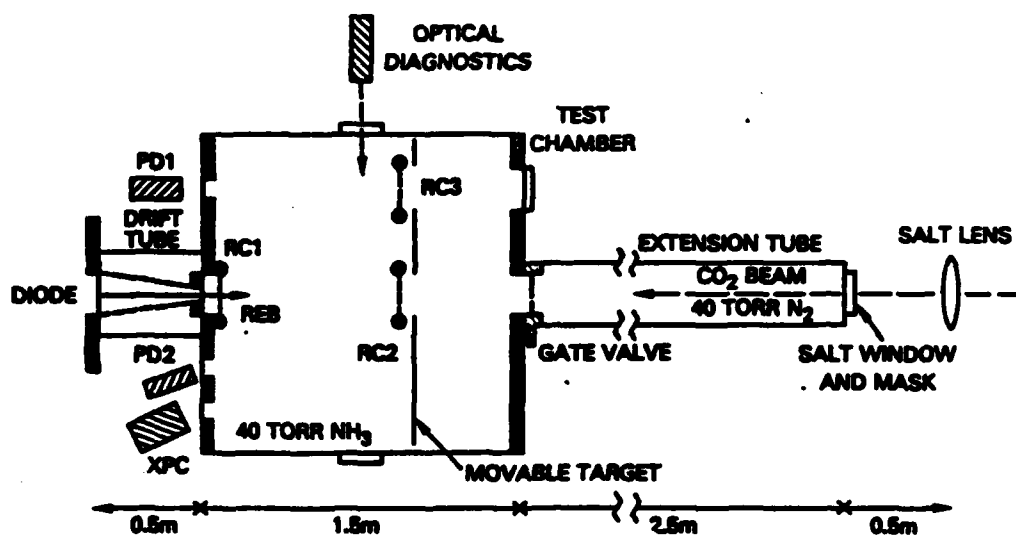
Figure 1

REB AND CHANNEL PROFILES

Figure 2

a) REB CURRENT I_B (kA)

b) NET CURRENT I_N (kA)

c) PLASMA CURRENT I_p (kA)

$I_p(t) = I_N(t) - I_B(t)$

Figure 3

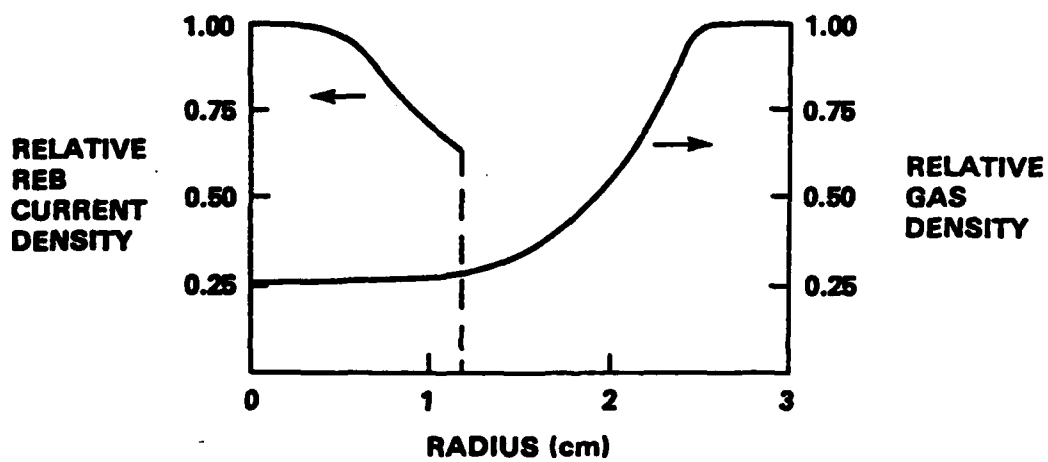IONIZATION RATES FOR AIR AND AMMONIA
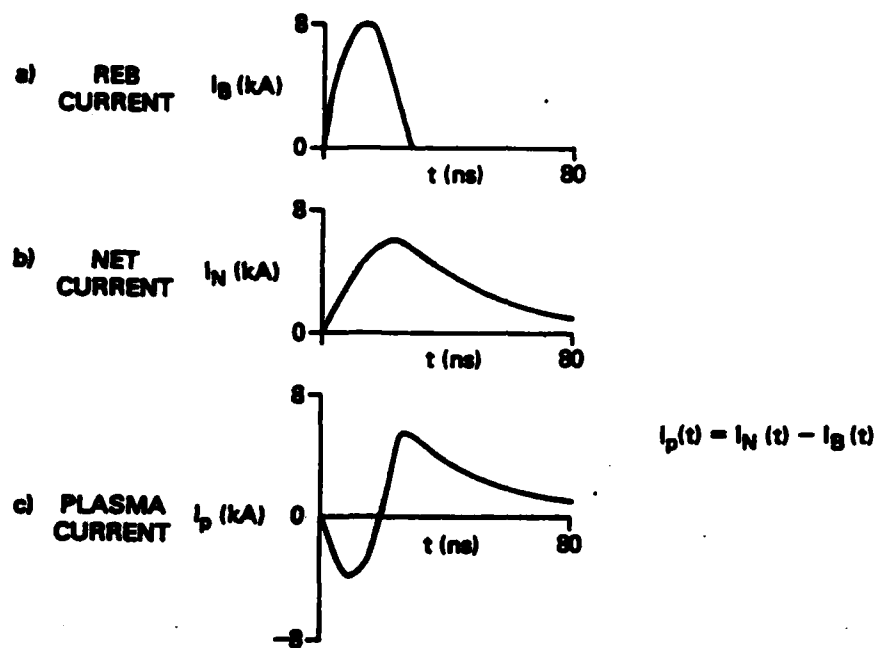
AIR

NH_3
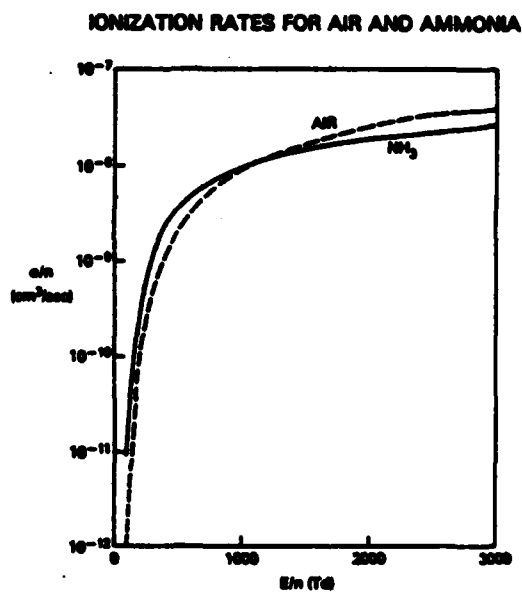
α/n (cm³/sec)

E/n (Td)

Figure 4

REFERENCES

1. G. Herzberg, <u>Electronic Spectra and Electronic Structure of Polyatomic Molecules</u>, D. van Nostrand Co., New York, (1966), p. 609.
2. J.N. Olsen, J. Appl. Phys., <u>52</u>, 3279 (1981).
3. A.W. Ali, NRL Memorandum Report #5150 (1983). (AD-A131 591)
4. F.C. Jahoda in <u>Modern Optical Methods in Gas Dynamic Research</u>, edited by D.S. Dosanjh, Plenum Press, New York (1971), p. 137.
5. R.E. Pechacek, et al., NRL Memorandum Report #5277 (1984). (AD-A139286)
6. A.W. Ali, NRL Memorandum Report #4794 (1982). (AD-A113501)